SHEAR BANDING CHARACTERISTICS OF SAND IN TORSIONAL SHEAR TEST EVALUATED BY MEANS OF IMAGE ANALYSIS TECHNIQUE

Seto WAHYUDI[1], Yukika MIYASHITA[2] and Junichi KOSEKI[3]

ABSTRACT: Accurate measurement in shear banding and strain localization studies is critical in characterizing the microstructural behavior within failure area. This research is aimed to investigate the effects of initial relative density on the shear banding behavior of sand. A series of tests on Toyoura sand with different initial relative densities were conducted using a hollow cylinderical torsional shear apparatus under drained condition. Unlike the tests conducted on prismatic specimens on plane strain condition, the tests conducted on hollow cylinderical specimens require more complex data analysis due to the curvature of their outer side surface. Therefore, this paper introduces as well a special image analysis method to convert the local movements of target points on the curved surface into those on a virtual flat surface. The test results show that shear band is initiated around peak stress state and the inclinations of shear band obtained by image analysis in all tests are located lower than those predicted by Coulomb's formulation. Both dilatancy rate and shear band expansion magnitude are found to have unique relationships with the specimen initial relative density.

Key words: Shear band, relative density, dilatancy, torsional shear, shear band angle, shear displacement and shear band extension.

INTRODUCTION

One of the important phenomenons associated with the microstuctural behavior within failure area in geomechanics is so called shear banding or stain localization. Shear banding process is initiated at the state when the mobilized strength of geomaterial reaches its peak and develops as shear deformation continues. Researchers have found that shear banding and strain localization behaviors were affected by various parameters such as particle mean diameter, confining stress among others.

Shear band observation in laboratory test suffers drawback due primarily to the requirement to employ tools with high accuracy and complex analysis. Therefore, researchers proposed and developed their own methods by various means. Harris et al. (1995) among others used stereophotogrammetry techniques to observe the distribution and development of voids along the shear band. Sadrekarimi and Olson (2010) among others used particle velocimetry technique in which single particle movements through the transparent media can be tracked. However, perhaps the most common technique used in this field is image-processing technique. Yoshida et al. (1994) investigated how the thickness of shear band was affected by various parameters. Image processing technique offers a practical solution to employ in laboratory test while at the same time enables to obtain high accuracy of measurements, thanks to the recent advancement in imaging/optical researches.

[1] Graduate Student, Department of Civil Engineering, The University of Tokyo
[2] Technical Assistant, Institute of Industrial Science, The University of Tokyo
[3] Professor, Institute of Industrial Science, The University of Tokyo

Recent studies on shear banding and strain localization were mostly conducted in plane strain compression test. However, in this paper, shear banding observations were conducted by using hollow cylinder torsional shear apparatus. Unlike plane strain compression test, torsional shear apparatus is capable of simulating the rotation of major principal stress direction during loading process. However, shear banding observation in torsional shear test may complicate the analysis process due to the cylindrical specimen surface.

Limited numbers of researches that are related with shear banding studies have been conducted by using torsional shear apparatus. Therefore, this paper is aimed to investigate the effects of relative density on shear banding of sand while at the same time providing special image analysis method that can be used in torsional shear test.

EXPERIMENTAL PROGRAM

Toyoura sand was used as the test material. Its particles have an angular or sub-angular shape with the following physical properties: specific gravity, G_s=2.656; mean diameter, D_{50}=0.162mm; fines content, F_c=0.1%; max. void ratio, e_{max}=0.992; min. void ratio, e_{min}=0.632. Tests were conducted on hollow cylindrical specimen, as shown in Fig. 1, having the height of 30cm, the inner and outer diameters of 12cm and 20cm, respectively.

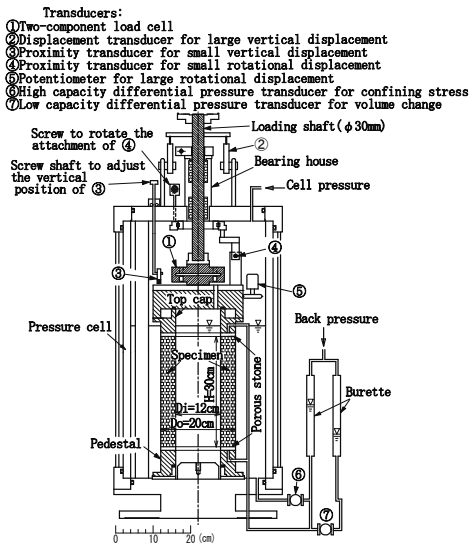

Figure 1. Hollow cylindrical torsional shear appartus

A series of test were conducted under different values of initial relative density at Dr_0= 53.9% (e_0=0.779), Dr_0= 73.2% (e_0=0.710) and Dr_0= 81.7% (e_0=0.680), which correspond to loose, medium dense and dense packing. Specimens were prepared by pluviation of air-dried sand particles into a mold through air. Their falling height was kept constant throughout the pluviation process in order to obtain specimens with highly uniform density. To satisfy fully saturated condition (B-value $\geq$ 0.96), double vacuuming was used during the saturation process, considering the large size of the specimen.

A drained shear loading with constant shear strain rate of 0.15 %/min. was applied while maintaining other stresses at $\sigma_z'=\sigma_r'=\sigma_\theta'$= 100 kPa throughout the loading process. Finally, the loading process was terminated when the global shear strain achieved 20%.

For the image analysis purpose, black dots of about 1.0 mm in diameter were pasted at a constant spacing of 5mm x 5mm on the front face of outer membrane covering the specimen. A digital camera

with the resolution of 3456 x 2304 pixels was employed to take a series of digital photos. The photo-taking timer was regulated by the control system connected via D/A board to the computer as shown in Fig. 2. During torsional shear loading, each photo was taken at a constant interval time of 1 minute, which corresponds to 0.15% in terms of global shear strain increment ($d\gamma$). In addition, to enhance the contrast between the black-colored target dots and bright color of membrane, two sets of light sources were prepared on each side of torsional shear apparatus.

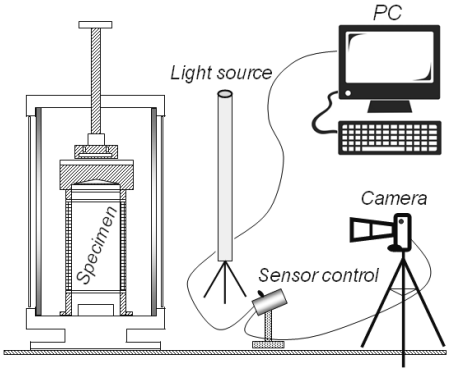

Figure 2. Configuration of photo control system

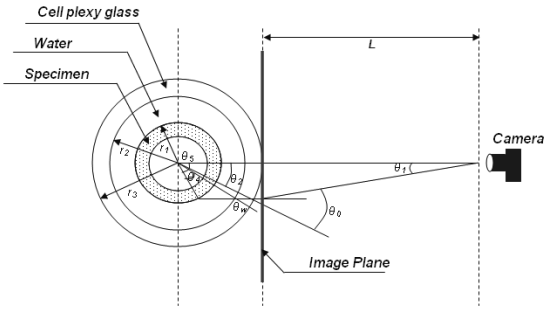

Figure 3. Plan view of configuration image taken by the camera

DATA ANALYSIS PROCEDURE

As shown in Fig. 3, the digital camera transforms three-dimensional object into two-dimensional image as projected on the image plane. As a result, cylindrical surface of the specimen in hollow cylinder apparatus would create so called warping distortion on the image plane. In addition, the refraction of water inside the cell chamber and the possibility of unsymmetrical initial setting of the camera would enhance the distortion.

In analyzing the image, the apparent orthogonal coordinates (x,y) from the target dots were tracked by an image tracking software (Move-tr/2D Ver. 7.21) with the accuracy of about 0.1mm. Then, correction is applied to convert the apparent coordinates into the real ones (x',y') as shown in Figs. 4(a) and 4(b). In this study, the correction functions were formulated using polynomial function as shown in Eq. 1 below.

$$x' = f_1(x,y) \quad \& \quad y' = f_2(x,y)$$
$$x'_{(m)} = a_{0(m)}.1 + a_{1(m)}.x_{(m)} + a_{2(m)}.y_{(m)} + a_{3(m)}.x^2_{(m)} + a_{4(m)}.x.y_{(m)} + a_{5(m)}.y^2_{(m)} \tag{1}$$
$$y'_{(n)} = b_{0(n)}.1 + b_{1(n)}.x_{(n)} + b_{2(n)}.y_{(n)} + b_{3(n)}.x^2_{(n)} + b_{4(n)}.x.y_{(n)} + b_{5(n)}.y^2_{(n)}$$

where, x' and y' are the real coordinates in horizontal and vertical directions, respectively. x and y are the apparent coordinates in horizontal and vertical directions, respectively. The coefficients a_0 through a_5 and b_0 through b_5 are assigned based on calibration results by means of least square error method. m and n are the number of column and row, respectively.

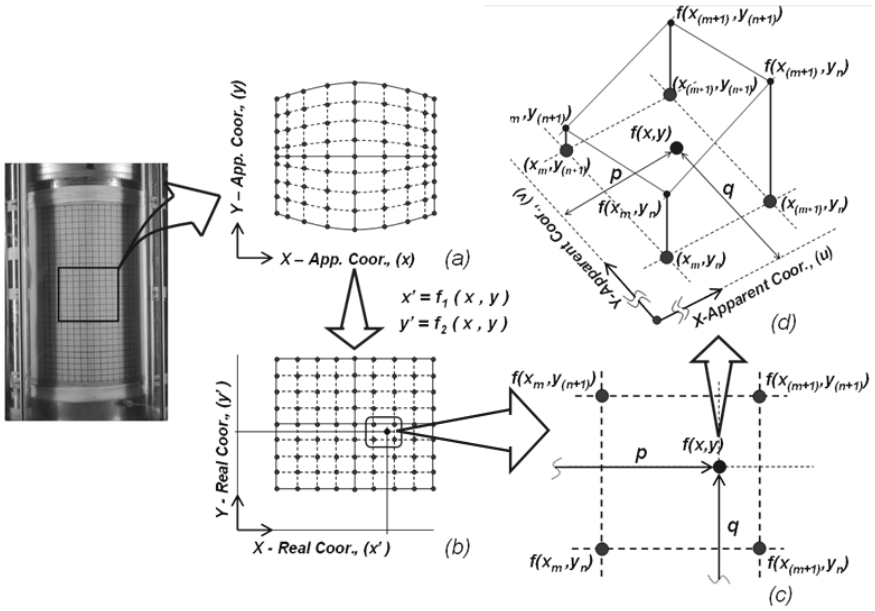

Figure 4. Image analysis procedure

In addition to the correction given above, the unknown real coordinate located in between other known coordinates is evaluated by using bilinear-interpolation method as shown in Figs. 4(c) and Fig. 4(d). Bilinear-interpolation method is generally used in optical/imaging engineering field to reduce visual distortion caused by fractional pixel. This method works by weighting the unknown value relative to their four known nearest-neighborhood values. The formulation of bilinear-interpolation method is given in Eq. 2:

$$
\begin{aligned}
(x', y') = f(x, y) = \quad & \frac{f(x_m, y_n)}{(x_{m+1} - x_m).(y_{n+1} - y_n)}.\{(x_{m+1} - p).(y_{n+1} - q)\} + \\
& \frac{f(x_{m+1}, y_n)}{(x_{m+1} - x_m).(y_{n+1} - y_n)}.\{-(x_m - p).(y_{n+1} - q)\} + \\
& \frac{f(x_m, y_{n+1})}{(x_{m+1} - x_m).(y_{n+1} - y_n)}.\{(x_{m+1} - p).-(y_n - q)\} + \\
& \frac{f(x_{m+1}, y_{n+1})}{(x_{m+1} - x_m).(y_{n+1} - y_n)}.\{-(x_m - p).-(y_n - q)\}
\end{aligned}
\tag{2}
$$

where, p and q are the apparent coordinates of random target point in horizontal and vertical directions, respectively.

The bilinear-interpolation method is effective in handling and also reducing the fractional distortions. In order to confirm the accuracy of this method, a calibration test was conducted by tracking several points attached on the moveable top cap while using the fixed pedestal as reference as shown in Fig. 5. Fig. 6 shows the tracking result of target points before correction (in symbols) and after correction (in thick line). The result shows that the displacements of all three target points corrected by the bilinear-interpolation method were similar to each other, while the uncorrected ones (raw data) were diverged as the points move away from their initial positions.

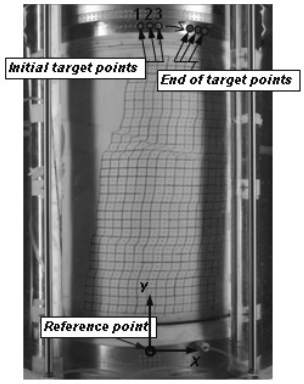

Figure 5. The calibration of image analysis method

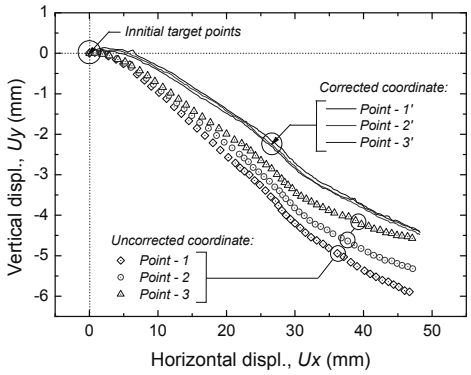

Figure 6. Calibration results of image analysis method

In this study, shear banding characteristics is presented in the form of relationship between shear displacement across the shear band (*Us*) and the change of shear band expansion (*Un*). Therefore, the evaluation of shear displacement (*Us*) and shear band expansion (*Un*) as well as the angle of shear band (θ) will be discussed as follows.

Evaluation of shear band angle (θ): In torsional shear test, shear band is formed in a spiral shape with a certain inclination angle. Shear band angle was evaluated by measuring both vertical and horizontal distances between two observation points (H and L) located across the shear band as shown in Fig. 7.

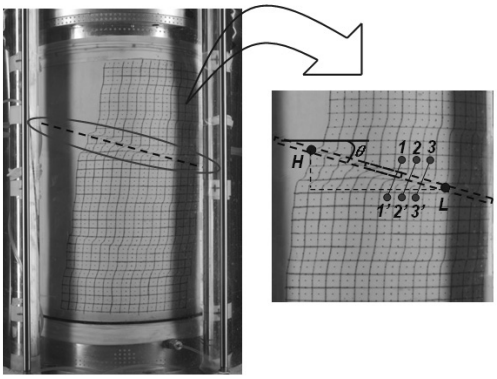

Figure 7. Shear band inclination and image analysis observation target points

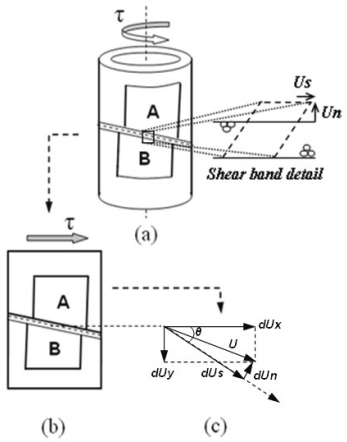

Figure 8. Shear band expansion (*Un*) and shear displacement (*Us*) evaluation procedures

Evaluation of shear displacement (*Us*) and shear band expansion (*Un*): Three pairs of target points located just outside of shear band were selected as shown in Fig. 7. Then, their relative displacements in parallel and perpendicular with the shear band (*dUs* and *dUn*, respectively) were evaluated as shown in Fig. 8. Finally, shear displacement (*Us*) and shear band expansion (*Un*) were obtained by integrating these increments. The accuracy of evaluation was confirmed by comparing the respective results from the three pairs of observation.

TEST RESULTS AND DISCUSSION

Global stress-strain and volumetric-strain relationship: Fig. 9 shows the global shear stress ratio-shear strain relationship, and Fig. 10 shows global volumetric strain-shear strain relationship. Both figures clearly show that denser specimens consistently achieve higher peak of shear stress ratio $(\tau/p')_{peak}$ and higher positive dilatancy. It can be seen in the global volumetric strain-shear strain relationship that the dilatancy rate remains positive during the post-peak strain softening region and even at the residual stress states; however, this behavior is different from the local behavior within the shear band as discussed later.

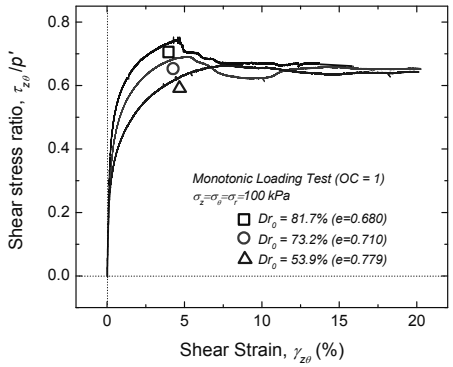

Figure 9. Global shear stress-shear strain relationship

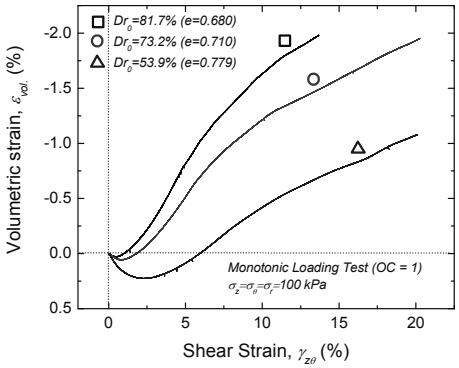

Figure 10. Volumetric strain-shear strain relationship

Yoshida et al. (1994) revealed the shear banding process is initiated near to the peak stress state and develops through the residual stress states. Therefore, shear displacement and shear band expansion in the post-peak stress state region are evaluated as $Us^* = Us-(Us)_{peak}$ and $Un^* = Un-(Un)_{peak}$, respectively, where $(Us)_{peak}$ and $(Un)_{peak}$ are the values of Us and Un at the peak stress state.

In the following figures, shear band deformation (Us^* and Un^*) are presented in their relation with shear stress level (Rn), where shear stress level itself is defined in Eq. 3 as shown below.

$$Rn = \frac{(\sigma_1/\sigma_3)-(\sigma_1/\sigma_3)_{res}}{(\sigma_1/\sigma_3)_{peak}-(\sigma_1/\sigma_3)_{res}} \tag{3}$$

where, σ_1 and σ_3 are the major and minor principal stresses, respectively, $(\sigma_1/\sigma_3)_{res.}$ is the stress ratio at residual state and $(\sigma_1/\sigma_3)_{peak}$ is the stress ratio at peak state.

Shear displacement (Us): Fig. 11(a) shows the stress level (Rn) and shear displacement (Us^*) relationship. From the peak stress state ($Rn=1$) to the residual stress state ($Rn=0$), the dense and medium dense specimens attained shear displacement of around 2 mm and 4 mm, respectively, while the loose specimen attained much larger shear displacement of around 8 mm. Smaller gains of shear displacement with the denser specimens in this post-peak strain softening region were possibly caused by more abrupt decrease of their shear stresses as shown in Fig. 9.

Shear band expansion (Un): Fig. 11(b) shows the stress level (Rn) and shear band expansion (Un^*) relationship. It can be noted that, all the three specimens attained initial expansion of about 0.5 mm - 1.0 mm immediately after peak stress state ($Rn\approx1$), followed by progressive change in the expansion rate during the post-peak strain softening region. Han and Drescher (1993) among others reported similar phenomenon in which large rate of increase in the shear band thickness (positive dilatancy) occurred immediately after the onset of shear band formation.

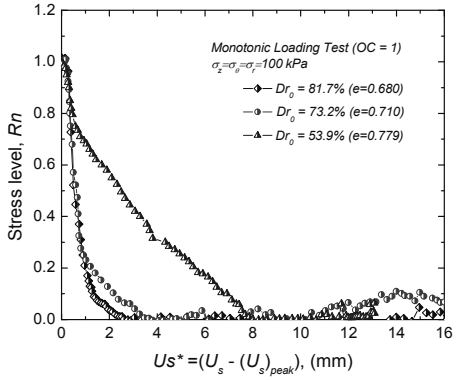

Figure 11(a). Stress level-shear displacement relationship

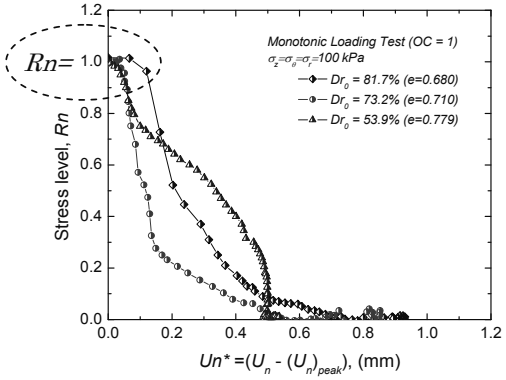

Figure 11(b). Stress level-shear band expansion relationship

By combining the results shown in Fig. 11(a) and Fig. 11(b), the shear displacement (*Us**) and shear band expansion (*Un**) relationship is plotted in Fig. 12. Shortly after the onset of shear band formation around the peak stress state, the shear band expanded rapidly and then at some point the expansion rate (=*dUn/dUs*) was decreased towards zero. The latter local behavior in shear band was found to be different from their global behavior as previously discussed. It is also observed that the shear band subsequently exhibited slight contraction.

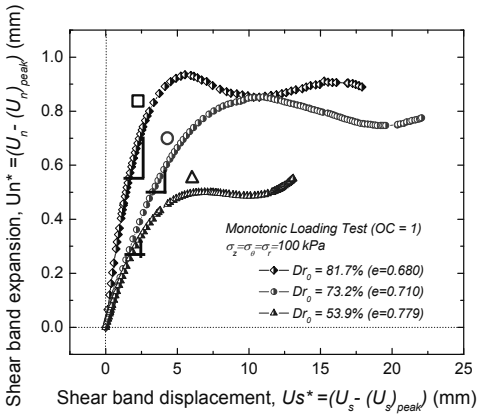

Figure 12. Post peak shear band expansion-shear displacement relationship

Figure 12 also suggests that initial relative density of specimen affects the behavior of shear band. First, denser specimens initially exhibited higher expansion rate (positive dilatancy). Second, denser specimen reached larger amount of shear band expansion. In the current tests, the dense and medium dense specimens reached expansion of approximately 0.9 mm and 0.8 mm, respectively, while the loose specimen reached expansion of approximately 0.5 mm. Similar findings have been reported by Yoshida et al. (1994), where the final value of shear band expansion (*Un*) is found to depend on the initial relative density.

CONCLUSIONS

The investigation of local behavior within the shear band and the global behavior of sand in torsional shear test revealed several observations, as summarized below:

1. The expansion rate (*dUn/dUs*) within the shear band is affected by the specimen initial relative density. Specimen with higher initial relative density shows higher rate.
2. The final value of shear band expansion (*Un*) depends on the specimen initial relative density, where denser specimen shows higher expansion.
3. The global behavior of specimen is slightly different from their local behavior within shear band. During the post-peak strain softening and residual stress state regions, the global behavior shows continuously positive dilatancy rate, while the local behavior shows decrease in the expansion rate of shear band that is followed by slight contraction.

ACKNOWLEDGEMENT

The authors would like to thank Mr. Takeshi Sato (Technical assistant in Geotechnical Engineering lab, IIS) for his contribution in assembling the photo-taking control system for this research and operating the testing apparatus.

REFERENCES

Han, C. and Drescher, A. (1993). "Shear bands in biaxial tests on dry coarse sand". *Soils and Foundations*, Vol. 33. No. 1, pp. 118-132.

Harris, W. W., Viggiani, G., Mooney, M. A. and Finno, R. J. (1995). "Use of stereophotogrammetry to analyze the development of shear bands in sand". *Geotechnical Testing Journal* 18 (4). pp. 405 – 420.

Sadrekarimi, A. and Olson, S. A. (2010). "Shear band formation observed in ring shear tests on sandy soils". *Journal of Geotechnical and Geoenvironmental Engineering*, ASCE.

Yoshida, T., Tatsuoka, F., M. S. A. Siddiquee, Kamegai, Y. and C. S. Park (1994). "Shear banding in sands observed in plane strain compression". *In R Chambon, J Desrues, I. Vardoulakis (eds). Localization and Bifurcation Theory for Soils and Rocks*: 165 – 179. Balkema: Rotterdam.

Yoshida, T. and Tatsuoka, F., 1997. "Deformation property of shear band in sand subjected to plane strain compression and its relation to particle characteristics". *Proceedings of 14th International Conference of Soil Mechanics and Foundation Engineering*, Hamburg, pp. 237 – 240.